A photosynthetic antenna complex foregoes unity carotenoid-to-bacteriochlorophyll energy transfer efficiency to ensure photoprotection

Dariusz M. Niedzwiedzki[a,b,1], David J. K. Swainsbury[c], Daniel P. Canniffe[d], C. Neil Hunter[c], and Andrew Hitchcock[c,1]

[a]Center for Solar Energy and Energy Storage, Washington University in St. Louis, St. Louis, MO 63130; [b]Department of Energy, Environmental & Chemical Engineering, Washington University in St. Louis, St. Louis, MO 63130; [c]Department of Molecular Biology and Biotechnology, University of Sheffield, Sheffield S10 2TN, United Kingdom; and [d]Institute of Integrative Biology, University of Liverpool, Liverpool L69 7ZB, United Kingdom

Edited by Krishna K. Niyogi, University of California, Berkeley, CA, and approved February 6, 2020 (received for review November 27, 2019)

Carotenoids play a number of important roles in photosynthesis, primarily providing light-harvesting and photoprotective energy dissipation functions within pigment–protein complexes. The carbon–carbon double bond (C=C) conjugation length of carotenoids (*N*), generally between 9 and 15, determines the carotenoid-to-(bacterio)chlorophyll [(B)Chl] energy transfer efficiency. Here we purified and spectroscopically characterized light-harvesting complex 2 (LH2) from *Rhodobacter sphaeroides* containing the $N = 7$ carotenoid zeta (ζ)-carotene, not previously incorporated within a natural antenna complex. Transient absorption and time-resolved fluorescence show that, relative to the lifetime of the S_1 state of ζ-carotene in solvent, the lifetime decreases ∼250-fold when ζ-carotene is incorporated within LH2, due to transfer of excitation energy to the B800 and B850 BChls *a*. These measurements show that energy transfer proceeds with an efficiency of ∼100%, primarily via the $S_1 \rightarrow Q_x$ route because the $S_1 \rightarrow S_0$ fluorescence emission of ζ-carotene overlaps almost perfectly with the Q_x absorption band of the BChls. However, transient absorption measurements performed on microsecond timescales reveal that, unlike the native $N \geq 9$ carotenoids normally utilized in light-harvesting complexes, ζ-carotene does not quench excited triplet states of BChl *a*, likely due to elevation of the ζ-carotene triplet energy state above that of BChl *a*. These findings provide insights into the coevolution of photosynthetic pigments and pigment–protein complexes. We propose that the $N \geq 9$ carotenoids found in light-harvesting antenna complexes represent a vital compromise that retains an acceptable level of energy transfer from carotenoids to (B)Chls while allowing acquisition of a new, essential function, namely, photoprotective quenching of harmful (B)Chl triplets.

photosynthesis | carotenoids | light-harvesting | photoprotection | ultrafast spectroscopy

Carotenoids (Cars) are natural pigments found in plants, algae, and photosynthetic (cyano)bacteria where they function in light-harvesting, stabilization of pigment–protein complex structure, and photoprotection (1, 2). In antenna complexes and photosystems, Cars act as accessory light-harvesting pigments and transfer excitation energy to (bacterio)chlorophylls [(B)Chls]. The absorption bands of Cars typically span the 400 to 550 nm spectral range and are associated with the $S_0 \rightarrow S_2$ electronic transition of the linear carbon–carbon double bond (C=C) conjugation (N), a characteristic structural motif (3, 4). Cars also serve important photoprotective functions in light-harvesting complexes, typically quenching harmful excited triplet states of (B)Chls to inhibit formation of reactive oxygen species such as singlet oxygen (5). The photophysical properties of Cars and their roles in numerous light-harvesting antennas have been investigated (6). The LH2 complex from purple photosynthetic bacteria has been a model antenna for such studies (7–16) as crystal structures are available (17, 18), the Car content can be manipulated (14, 19–22), and its relatively simple pigment composition reduces the number of features that must be interpreted in spectroscopic analyses.

Numerous studies have shown that the Car-to-BChl *a* energy transfer efficiency ($\Phi_{Car \rightarrow BChl}$) varies in LH2s from different purple bacterial species and appears to correlate with the Car conjugation length. The yields for Cars such as neurosporene ($N = 9$) or spheroidene ($N = 10$) are 85 to 95% (11, 19, 23–25). The yields decrease to 55 to 65% for Cars where $N = 11$ (e.g., rhodopin, rhodopin glucoside, or lycopene) (11, 24–26) and reduce further to ∼30% when $N = 13$ (spirilloxanthin) (14). As longer C=C conjugation length (larger N) lowers the energies of both the S_2 and S_1 excited states (2, 6), the broadly accepted explanation for the variation in $\Phi_{Car \rightarrow BChl}$ in LH2 is linked with the inherent excited-state properties of the particular Car. Typically, both S_2 and S_1 states are involved in energy transfer to BChls, and if the S_1 state falls below the Q_y bands of the B800 and B850 spectral forms of BChl *a*, reducing spectral overlap of the hypothetical S_1 emission and BChl *a* absorption, then the $\Phi_{Car \rightarrow BChl}$ declines sharply. At first glance, some Cars do not appear to fit into this correlation, for example, okenone with $N = 13 + C=O$, where nominally there are 13 conjugated carbon–carbon

Significance

Photosynthesis uses carotenoids as light-harvesting pigments and for photoprotective energy dissipation. The carbon–carbon double bond conjugation length of carotenoids (*N*) affects the carotenoid-to-(bacterio)chlorophyll energy transfer efficiency, but the photoprotective capability was considered to be independent of *N*. Using light-harvesting complex 2 from the model photosynthetic bacterium *Rhodobacter sphaeroides* containing ζ-carotene ($N = 7$) or neurosporene ($N = 9$), we demonstrate that decreasing the conjugation length increases the carotenoid-to-bacteriochlorophyll energy transfer efficiency, in the case of ζ-carotene to ∼100%. However, unity quantum efficiency comes at the cost of photoprotection, suggesting that naturally evolved photosynthesis tolerates some energetic loss to allow essential energy dissipation, explaining why longer-conjugation length carotenoids are utilized in native pigment–protein complexes.

Author contributions: D.M.N. and A.H. designed research; D.M.N., D.J.K.S., D.P.C., and A.H. performed research; D.M.N., D.J.K.S., D.P.C., C.N.H., and A.H. analyzed data; and D.M.N., D.J.K.S., D.P.C., C.N.H., and A.H. wrote the paper.

The authors declare no competing interest.

This article is a PNAS Direct Submission.

[1]To whom correspondence may be addressed. Email: niedzwiedzki@wustl.edu or a.hitchcock@sheffield.ac.uk.

This article contains supporting information online at https://www.pnas.org/lookup/suppl/doi:10.1073/pnas.1920923117/-/DCSupplemental.

First published March 5, 2020.

bonds and a terminal C=O group that could extend the conjugation length. Okenone bound within the LH2 complex from the bacterium *Merichromatium purpuratum* (formerly *Chromatium purpuratum*) shows $\Phi_{Car \rightarrow BChl}$ = ~86% (27), substantially above the expected value of ~30% observed for other $N = 13$ Cars. However, previous investigations have demonstrated that when conjugation is extended into the cyclic ends of Cars, the double bonds in the rings act as only ~0.3 of a double bond in the linear backbone, and in case of Cars with aryl rings such as okenone the contribution may be even smaller (28, 29). Indeed, it has been shown that the energies of the excited states of okenone are only marginally smaller than their counterparts for the open chain Car spheroidenone ($N = 10$ + C=O) (30), which when bound to LH2 shows a $\Phi_{Car \rightarrow BChl}$ of 92 to 94% (11, 20).

Unlike $\Phi_{Car \rightarrow BChl}$ efficiency, the ability to provide photoprotective quenching of BChl *a* excited states (triplets) is more or less the same for all of the above mentioned Cars incorporated into LH2 (7, 31, 32). It could therefore be perceived that the ability to photoprotect (B)Chls in photosynthetic antennas is a universal characteristic of all Cars; however, this is not the case. Energetic requirements between (B)Chl and Car triplet states must also be considered, and, like the S_2 and S_1 states, the triplet states of Cars have well-defined energies that also depend on N, although this is impossible to confirm directly due to undetectable phosphorescence. Interestingly, photosynthetic organisms have a strong preference for Cars with $N \geq 9$ for incorporation into light-harvesting proteins (1), suggesting that these Cars have triplet state energies in a sweet spot corresponding to the triplet state energies of specific (B)Chls to ensure the most efficient sensitization [(B)Chl triplet quenching] (33). In support of this idea, experiments that tested photoprotective abilities of open chain and cyclic Cars of different N lengths in Car–Chl *a* model mixtures demonstrated that photoprotective capability appears to fall sharply for Cars with $N \leq 8$ (34–36).

Here we set out to better understand the relationship between Car conjugation length, Car-to-BChl energy transfer efficiency, and Car photoprotective ability using LH2 complexes from the model purple phototrophic bacterium *Rhodobacter sphaeroides* containing either neurosporene ($N = 9$) or ζ-carotene ($N = 7$). Using this model antenna we provide direct evidence that Cars with a conjugation length of only 7 are fully efficient in Car-to-BChl *a* energy transfer but are unable to quench BChl *a* triplets, a conflict that could have influenced the evolution of a compromise between energy transfer and photoprotection in light-harvesting complexes from other phototrophic organisms.

Results

ζ-Carotene to BChl *a* Energy Transfer in LH2 Proceeds with Unity Quantum Efficiency. We performed comparative spectroscopic studies of ζ-carotene bound to LH2 (see *Materials and Methods* and *SI Appendix*, Fig. S1, for details of the ζ-carotene–producing strain of *R. sphaeroides* and purification of LH2) and isolated ζ-carotene in solvent; steady-state absorption in both environments and the fluorescence emission spectra of ζ-carotene in solvent and LH2 in buffer are shown in Fig. 1. The absorption spectrum of LH2-bound ζ-carotene shows two clearly pronounced vibronic bands at 441 and 413 nm. The near-perfect overlap of the absorptance (1-transmittance) and the fluorescence excitation spectra when monitoring emission exclusively from BChl *a* shows that ζ-carotene is a perfect excitation energy donor to BChl *a* with $\Phi_{Car \rightarrow BChl}$ ~ 100% (Fig. 1*A*). This ideal Φ value suggests that there are no additional processes competing with energy transfer (ET), such as triplet formation via singlet fission or formation of a Car cation, which reduces $\Phi_{Car \rightarrow BChl}$ by 5 to 15% for Cars with longer N values (11, 21, 37). Examination of the spectra reveals that the S_2 excited state is too far from the Q_x absorption resulting in insufficient overlap to permit $S_2 \rightarrow Q_x$ energy transfer. Transfer from $S_2 \rightarrow Q_x$ is typical for Cars with longer conjugations (i.e., S_2 energies red shifted relative to that

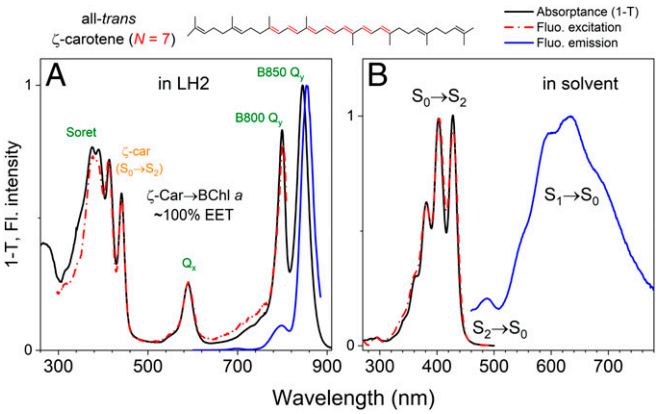

Fig. 1. Spectroscopic comparison of the ζ-carotene–containing LH2 antenna complex from *R. sphaeroides* and all-*trans*-ζ-carotene in solvent at room temperature. The chemical structure of all-*trans*-ζ-carotene is shown above the panels. The C=C bonds highlighted in red indicate the conjugation length ($N = 7$) of the Car. (*A*) Comparison between absorptance (black) and fluorescence excitation (red) spectra shows that, in LH2, ζ-carotene transfers excitation energy to BChl *a* essentially without any energetic loss. (*B*) All-*trans*-ζ-carotene dissolved in solvent shows pronounced fluorescence emission from the S_1 state and a much weaker emission band from the S_2 state.

of ζ-carotene) (10); therefore, it is possible that the majority of the ET occurs from the S_1 excited state. It is broadly accepted that LH2 complexes bind Cars in all-*trans* geometry (17), and for comparative studies with isolated Car in solvent, we purified the all-*trans* geometric isomer of ζ-carotene (the purification procedure is described in *SI Appendix*, Fig. S2). To examine the intrinsic properties of the all-*trans*-ζ-carotene S_1 state, we combined steady-state and time-resolved fluorescence (TRF) measurements with transient absorption (TA) spectroscopy. As demonstrated in Fig. 1*B*, the Car dissolved in solvent has detectable fluorescence. We assign the main band between 550 and 700 nm as emission from the $S_1 \rightarrow S_0$ transition and the smaller band at ~480 nm as emission from $S_2 \rightarrow S_0$. Generally, Cars are known to have very low fluorescence quantum yields; therefore, the fluorescence spectrum could easily be overwhelmed by sample contaminants. To ensure that the emission is associated with the Car fluorescence the excitation spectrum was measured (Fig. 1*B*, red dash-dotted line). The very good agreement with the absorptance (1-transmittance) spectrum of all-*trans*-ζ-carotene confirms that the observed emission is that of the $S_1 \rightarrow S_0$ fluorescence emission of the Car.

ζ-Carotene to BChl *a* Energy Transfer Proceeds from the S_1 Excited Singlet State. The fluorescence spectra show that emission from the S_1 and S_2 transitions partially overlap, and it is uncertain if the vibronic band at ~550 nm originates from the S_1 excited state (0-0 vibronic band) or if an additional peak at shorter wavelengths is obscured by the tail of the S_2 state emission. Using TRF of the Car, as shown by the pseudocolor 2D fluorescence decay contour map in Fig. 2*A*, we could unambiguously assign these features. It is clear that both emissive transitions are temporally resolved. What is not apparent from the contour is that there is a weaker, longer-lived band with a maximum at ~550 nm that is likely associated with emission from sample contaminants, which may form and accumulate during laser exposure. Global analysis of the TRF data was used to temporally and spectrally separate emission bands; Fig. 2*B* shows these results along with the kinetic scheme used for fitting. The fitting results (species associated spectra [SAS]) reflect emission from the excited states of the Car and sample contaminants. Fitting shows that the intrinsic lifetime of the S_1 state is 340 ps. The quality of the fit is shown in Fig. 2*C*, which contains the

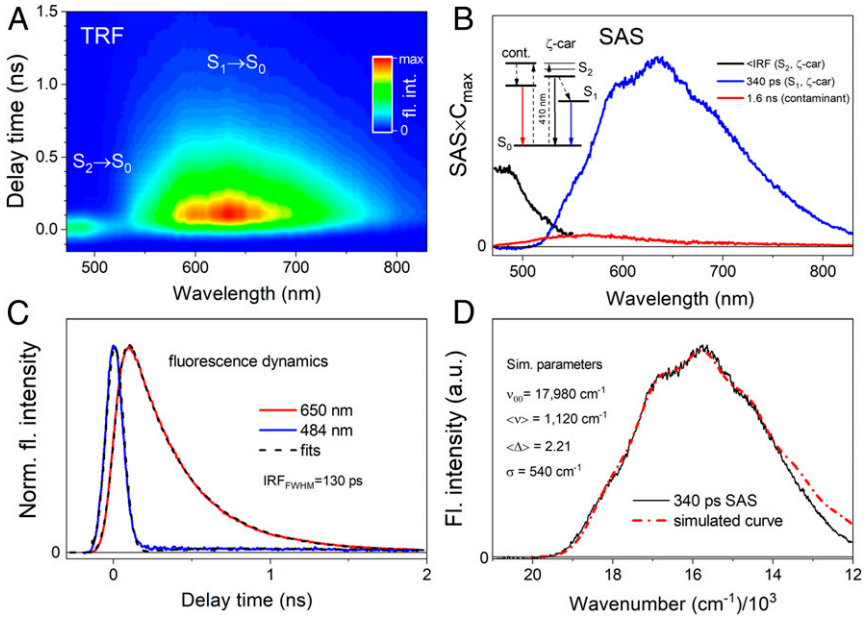

Fig. 2. TRF of all-*trans*-ζ-carotene in solvent upon excitation at 410 nm at room temperature. (*A*) Pseudocolor contour of TRF with the $S_2 \rightarrow S_0$ and $S_1 \rightarrow S_0$ transitions indicated. (*B*) Global analysis results (SAS) from application of fitting the model depicted in the panel. The SAS are normalized to their maximal time-dependent concentrations. A small contribution of the long-lived (1.6-ns) component was also necessary to properly fit the TRF data, which most likely originates from a decomposition product that slowly accumulates during measurements. (*C*) Fluorescence dynamics for two exemplary wavelengths accompanied with fits. (*D*) Simulation of the $S_1 \rightarrow S_0$ fluorescence spectrum, approximated by the 340-ps SAS from *B*, with FC progression. For more details please refer to the text. Simulation places the S_1 state energy at ∼18,000 cm^{-1} (555 nm).

fluorescence decay profiles for the S_1 and S_2 states together with fits from global analysis. In order to obtain the S_1 state energy from the fluorescence emission, the 340-ps SAS was subjected to a simulation of the vibronic progression with Franck–Condon (FC) factors according to a simplified formula that assumed only one average vibronic mode <ν> contributing to the spectrum with an average displacement <Δ> between the state coordinates (Fig. 2*D*) (see *Materials and Methods* for more details). The simulated spectrum (red line) was obtained based on the following parameters: υ = 6 (number of vibronic bands), <Δ> = 2.21, <ν> = 1,120 cm^{-1}, ν_{00} = 17,980 cm^{-1} (energy of the S_1 state), σ = 540 cm^{-1} (width of the vibronic band), and C = 72 (arbitrary scaling constant).

To permit comparison with the LH2-bound Car, the excited state lifetime of all-*trans*-ζ-carotene in solvent was also determined by TA spectroscopy. The TA results obtained at room temperature and 77 K, along with an expanded description, are provided in *SI Appendix*, Fig. S3. Fitting of the TA data gives an S_1 state lifetime of 340 ps, in excellent agreement with the TRF measurements despite the vastly different temporal resolutions of the two methods. The extensive overlap of the ζ-carotene emission spectrum with the 600-nm BChl *a* Q_x absorption, combined with its strong fluorescence emission (i.e., high quantum yield) and long S_1 excited state lifetime, should make ζ-carotene an ideal accessory light-harvesting pigment. We predict that ζ-carotene will perform better than its counterparts with longer conjugations such as neurosporene (N = 9) or spheroidene (N = 10), which show much weaker, almost undetectable $S_1 \rightarrow S_0$ fluorescence emission and have no spectral overlap with the BChl *a* Q_x band (38).

Dynamics of Car S_1 → BChl *a* Q_x Excitation Energy Transfer. To determine the excited state properties of ζ-carotene bound within LH2, TA spectroscopy was applied to the entire complex allowing simultaneous measurement of ζ-carotene and the energy-accepting BChls *a* (Fig. 3). Fig. 3*A* shows a pseudocolor 2D contour map measured between 330 and 910 nm over 1,300 ps plotted on a semilogarithmic time axis for better visibility of the transient bands. A subset of representative TA spectra taken at various times after excitation is shown in Fig. 3*B*, and dynamics at chosen wavelengths are shown in Fig. 3*C*. It is evident that the excited state absorption (ESA) band associated with the S_1 state (positive band at 489 nm) decays almost entirely within 4 ps. Given that the S_1 state lifetime in solvent is 340 ps, this dramatic reduction shows the high efficiency of the $S_1 \rightarrow Q_x$ route in the energy transfer process.

More details of the ET dynamics were revealed with global analysis of the TA data provided in Fig. 3*D*. Fitting was performed according to a sequential pathway of excitation decay and migration (irreversible steps from the fastest to the slowest lifetimes) to generate evolution associated decay spectra (EADS). This analysis does not necessarily reproduce the transient spectra of each species in the pathway, but it is satisfactory for obtaining macroscopic rates (observed lifetimes) of each distinct spectral component. These EADS can be interpreted by comparison with previous studies of other LH2 complexes. The EADS with a lifetime of 220 fs can be assigned to decay of the initially excited ζ-carotene S_2 state. The lifetime is similar to the S_2 lifetime observed in solvent at room temperature (*SI Appendix*, Fig. S3), which suggests that there is negligible ET to BChl *a*, and the excitation internally converts to the S_1 state. The S_1 state has a lifetime of 1.37 ps, ∼250-fold less than the 340-ps lifetime in solvent, confirming that it participates in extremely efficient ET to the Q_x bands of both the B800 and B850 spectral forms of BChl *a*, as demonstrated by simultaneous bleaching of the B800 and B850 bands associated with depletion of BChls in the ground state. Two EADS are associated with BChls, the B800* → B850 energy transfer at 4.9 ps (following excitation of the B800 BChl *a* from the Car S_1 state) and the decay of the excited B850 BChl *a* at 850 ps, for which the excited state lifetime is known to be ∼1,000 ps (22, 31, 32, 37).

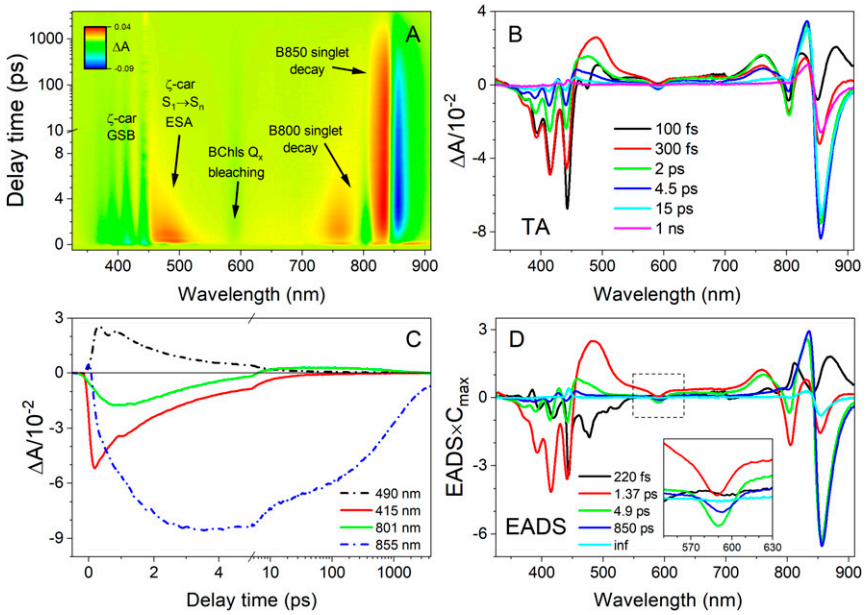

Fig. 3. Room temperature TA of ζ-carotene–containing LH2 from *R. sphaeroides* upon excitation of the Car absorption band. (*A*) The 2D pseudocolor contour of TA with spectral features marked. (*B*) Representative TA spectra taken at various delay times after excitation at the (0-0) vibronic band of the $S_0 \rightarrow S_2$ absorption of ζ-carotene. (*C*) Example TA time courses recorded at selected wavelengths. (*D*) EADS with application of a sequential decay model. (*Inset*) A zoomed-in view of the Q_x band. GSB, ground state bleaching.

ζ-Carotene Is Not a Quencher of BChl *a* Triplets. Fig. 3*D* shows a fifth EADS with an infinite (inf) lifetime, meaning it belongs to a process that is far slower than the 7-ns measurement time window. The long lifetime and spectral shape suggest that it is associated with the B850 BChl *a* triplet, formed by intersystem crossing at an efficiency of ∼30% (32). The presence of this component is interesting because it is well established that B850 BChl *a* triplets are rapidly quenched by sensitization of Car triplets, at most within a few tens of nanoseconds of formation (31, 32). The accumulation of BChl *a* triplets is potentially damaging as they may sensitize harmful singlet oxygen, whereas Car triplets are harmless as the triplet energy safely dissipates as heat. Therefore, triplet quenching by Cars provides an essential photoprotective function. The presence of a kinetic component corresponding to long-lived B850 BChl *a* triplets suggests that this essential photoprotective mechanism is absent in LH2 complexes containing ζ-carotene. To test this hypothesis the LH2 complexes with ζ-carotene and a control LH2 complex containing neurosporene ($N = 9$) were studied by TA in the microsecond time domain (Fig. 4). The control LH2 was isolated from a Δ*crtC* mutant of *R. sphaeroides*, described previously (19). Fig. 4 *A* and *B* shows 2D-pseudocolor TA contours with transient bands marked with arrows. These are accompanied by selected TA spectra (Fig. 4 *C* and *D*) at various delay times after excitation, with Fig. 4 *C* and *D*, *Insets*, showing the spectral range of the Car triplet transient band. It is apparent that for the ζ-carotene–containing LH2 the Car triplet spectrum is absent, whereas it can be clearly seen for the control complex with neurosporene. Conversely, the triplet state of B850 is long-lived in the ζ-carotene–containing complex, whereas it completely decays within ∼70 ns in the neurosporene-containing LH2. Taken together these data show that in the ζ-carotene–containing LH2 the B850 BChl *a* triplet state is not quenched by formation of a Car triplet, whereas Car triplet formation is observed in the control neurosporene-containing LH2 (compare Fig. 4 *E* and *F*).

Discussion

This study provides direct evidence that Cars with shorter conjugation lengths (here $N = 7$) are unable to participate in the essential function of photoprotection in a model bacterial light-harvesting complex. Triplet state energies of monomeric (B)Chls are already well defined and depending on the (B)Chl species span an energetic range of 8,000 to 10,750 cm^{-1} (930 to 1,250 nm). All these triplet states lie above the 7,870 cm^{-1} (1,270 nm) energy level of singlet oxygen (33), making them efficient sensitizers of this harmful product. Although the triplet energies of Cars cannot be measured directly due to a lack of spectral features, they can be inferred by their interactions with observable triplets of other molecules. Specifically, the triplet state of BChl *a* is ∼8,200 cm^{-1} (1,220 nm), marginally above singlet oxygen (33). Because Cars with $N \geq 9$ efficiently quench BChl *a*, this strongly suggests that they also have triplet energies below that of singlet oxygen, allowing efficient and harmless BChl *a* triplet quenching, as observed here in LH2 containing neurosporene. However, Cars with $N \leq 7$ are likely to have triplet energies above BChl *a* rendering triplet exchange to the Car energetically unfavorable, as observed here for LH2 containing ζ-carotene. In the absence of quenching, long-lived BChl *a* triplets will sensitize singlet oxygen leading to oxidative damage of the cell.

So what is the situation with Cars and N in other photosynthetic antenna complexes that use different species of B(Chl) for light-harvesting? As discussed above, the triplet state energy levels of the various (B)Chls that exist in nature span a broad energetic range; thus, the cutoff conjugation length at which Cars lose their photoprotective function in respect to a specific (B)Chl species may not be strictly limited to $N = 7$ in other light-harvesting complexes. However, because the triplet state of BChl *a* is energetically only marginally higher than that of singlet oxygen, the lack of quenching of BChl *a* triplets by ζ-carotene strongly suggests that the energy of the triplet state of ζ-carotene is higher than the energy level of singlet oxygen. Consequently, employing a Car with $N = 7$ (or less) in any LH complex is unlikely to be beneficial as even if the Car can quench a specific (B)Chl triplet, it will in turn become a singlet oxygen sensitizer itself.

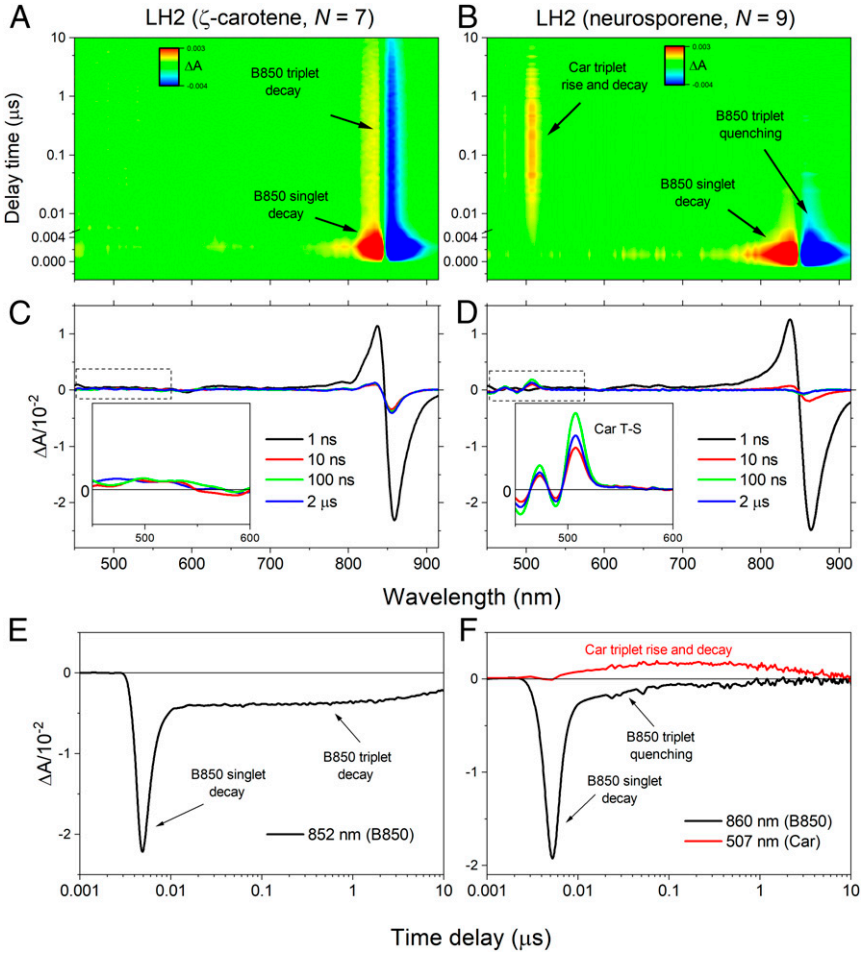

Fig. 4. TA of the ζ-carotene–containing LH2 complex over a microsecond time range and comparison with neurosporene-containing LH2. (*A* and *B*) Pseudocolor contours of the TA for both LH2 complexes obtained after excitation of the Car band. Noticeable transient bands are marked. (*C* and *D*) Individual TA spectra recorded at various delay times after the excitation. (*Insets*) TA in the spectral range in which triplet-minus-singlet (T-S) spectra of the Car appear. (*E* and *F*) Representative TA kinetic traces recorded at the bleaching of B850 Q_y band (852 and 868 nm) and at the maximum of the Car $T_1 \rightarrow T_n$ ESA band (507 nm, neurosporene-containg LH2 only). For clarity, time delays are plotted on a log scale and are slightly offset from $t_0 = 0$.

In summary, our study provides an insight into the coevolution of photosynthetic pigment–protein complexes and Car biosynthesis. Despite Cars with shorter conjugation length being simpler for the organism to produce, and their ability to transfer energy to (B)Chls with increased quantum efficiency, below a certain N value the inability to provide photoprotection of harmful B(Chl) excited states suggests it is not coincidental that all antenna complexes of photosynthetic organisms utilize Cars with $N \geq 9$.

Materials and Methods

Growth of *R. sphaeroides* and Generation of a ζ-Carotene–Producing Strain. Liquid cultures of *R. sphaeroides* were grown in M22+ medium (39) supplemented with 0.1% (wt/vol) casamino acids. For microoxic growth, cultures were shaken at 175 rpm at 30 °C. Phototrophic growth was performed in completely full culture vessels agitated with magnetic stir bars under ∼50 μmol photons m^{-2} s^{-1} illumination provided by OSRAM classic 116 W halogen bulbs. Media were supplemented with 30 μg mL^{-1} kanamycin and/or 10% (wt/vol) sucrose as appropriate.

The neurosporene-accumulating Δ*crtC* and phytoene-accumulating Δ*crtI* strains of *R. sphaeroides* 2.4.1 have been described previously (19); the *crtC* gene (rsp_0267) was deleted from the Δ*crtI* mutant using the pK18*mobsacB* allelic exchange construct described in the same study. The plasmid was conjugated into the Δ*crtI* strain from *Escherichia coli* S17-1 with selection on M22+ agar containing kanamycin. Subsequent plating on M22+ agar containing sucrose isolated colonies where the plasmid was excised from the genome and Δ*crtC* mutants were identified by PCR and verified by automated DNA sequencing.

To produce ζ-carotene in *R. sphaeroides*, the *Synechocystis* sp. PCC 6803 phytoene desaturase (PDS) encoding gene (*pds*, slr1254) was introduced to the Δ*crtI* Δ*crtC* background. The *pds* gene was amplified from genomic DNA with primers slr1254_F (5′-ACTG*AGATCT*ATGCGCGTTGTGATCGCC-3′; *Bgl*II site underlined in italics) and slr1254_R (5′-TCGA*CTCGAG*TTAACCCACGGTGACTATTTCCCTG-3′; *Xho*I site underlined in italics) using Q5 DNA polymerase (NEB). The resulting 1439 bp PCR product was digested with *Bgl*II/*Xho*I and ligated into the same sites of the replicative pBBRBB-*Ppuf843-1200* plasmid such that expression of *pds* is under control of the truncated *puf* promoter (40) The sequence verified plasmid was conjugated into the Δ*crtI* Δ*crtC* strain of *R. sphaeroides* from *E. coli* S17-1 with selection on M22+ agar containing kanamycin.

ζ-Carotene Extraction and Purification. Pigments (Cars and BChl *a*) were extracted with acetone and methanol at a 50:50 (vol/vol) ratio in a volume of ∼10 mL. Water (∼0.5 mL) was added, followed by ∼10 mL of petroleum ether. The mixture was agitated and saponified by adding a few small pellets of NaOH. Water was added until ζ-carotene was fully partitioned into the ether layer, which was carefully removed. The ether was dried down using a stream of nitrogen gas in darkness, and the Cars were resuspended in acetone. The mixture of ζ-carotene isomers was purified using an Agilent 1100 HPLC system consisting a quaternary pump, in-line diode array UV-Vis detector, and 4.6 × 250 mm Zorbax Eclipse XBD-C18 column. The flow rate was 1 mL/min, the sample injection volume was 100 μL (in acetone), and the mobile phase was 40:30:30 (vol/vol/vol) acetonitrile:methanol:tetrahydrofuran.

All-*trans*-ζ-carotene was isolated using a YMC Carotenoid C30 column with the same HPLC system, mobile phase and flow rate (see *SI Appendix* for more details). All solvents were HPLC grade (Millipore Sigma).

Purification of ζ-Carotene or Neurosporene Containing LH2. LH2 from the ζ-carotene or neurosporene producing strains was purified by ion-exchange and size-exclusion chromatography as described previously (41).

Spectroscopic Methods. Room temperature and 77 K steady-state absorption spectra of the LH2 complexes and isolated ζ-carotene were recorded using a UV-1800 spectrophotometer (Shimadzu). Fluorescence emission spectra of ζ-carotene and the LH2 samples were measured using an RF-6000 spectrofluorometer (Shimadzu) following excitation of the (0-0) vibronic peak of the $S_0 \rightarrow S_2$ absorption band of the Car dissolved in HPLC eluent (solvent mix; see above) and the Soret band of BChl *a* (370 nm), respectively. Excitation and emission bandwidths were set to 5 nm, and a 455-nm (650-nm) long-pass glass filter was used for emission measurements in solvent mix (LH2) at the detector entrance. Fluorescence excitation spectra were collected monitoring emission at 855 nm for LH2 and at 630 nm for the Car in solvent, with excitation and emission bandwidths of 5 nm. To minimize scattering effects, long-pass glass filters were placed at the detector entrance (610 nm for ζ-carotene in solvent mix and 780 nm for LH2). Cryogenic measurements at 77 K were carried out using a VNF-100 liquid nitrogen cryostat (Janis). ζ-carotene was dissolved in 2-methyltetrahydrofuran (2-MTHF) in a 1-cm cryogenic quartz cuvette (NSG Precision Cells) and slowly frozen in nitrogen vapor to form a transparent glass. For fluorescence studies all samples were adjusted to an absorbance of 0.1 at either the maximum of the $S_0 \rightarrow S_2$ absorption band (ζ-carotene) or the B850 band (LH2).

Room temperature and 77 K TA studies were performed using Helios and EOS, time-resolved pump–probe absorption spectrometers from UltrafastSystems. Pump and probe were provided by a Spectra-Physics femtosecond laser system described in detail previously (42). ζ-Carotene was dissolved in 2-MTHF and excited at 428 nm (room temperature) or at 439 nm (77 K). The LH2 complexes were excited at the (0-0) vibronic band of carotenoid absorption (442 nm for ζ-carotene and 489 nm for neurosporene). The excitation beam was focused on the sample in a spot of ∼1 mm diameter. The excitation energy was set to 200 to 400 nJ, corresponding to 6 to 1×10^{13} photons cm^{-2} $pulse^{-1}$.

TRF imaging studies were performed using a universal streak camera system from Hamamatsu (Hamamatsu Corporation) coupled to an excitation beam source in the form of an ultrafast laser system (Spectra-Physics) described previously (43). The repetition rate of the excitation laser beam was set to 8 MHz, and the beam was depolarized, focused on the sample in a circular spot of ∼1 mm diameter, and tuned to a wavelength of 410 nm, corresponding to second-order harmonics of 820 nm, produced in optical parametric oscillator. The photon flux of the excitation beam was $\sim 10^{10}$ photons cm^{-2} $pulse^{-1}$. Fluorescence emission was measured at right angle to the excitation beam (44). A long-pass 455-nm filter was placed at the entrance slit of the spectrograph to avoid scattering effects. Sample integrity was monitored in real time by observing photon count rate that, if constant, indicates stable signal and absence of sample photodegradation (44). In order to minimize sample decomposition, TRF studies were performed on the sample directly eluted from HPLC, without solvent exchange.

Data Processing and Global Analysis. Prior to analysis, TA datasets were corrected for temporal dispersion using Surface Xplorer 4.0 (UltrafastSystems LLC). The datasets were globally fitted with a kinetic model assuming a sequential population of excited states/species in a cascade of nonreversible, decreasing rates (longer lifetimes). The instrument response function (IRF) was simulated by a Gaussian with a full width at half-maximum (FWHM) of ∼200 fs. The fitting procedure applied to TA datasets gives EADS (45). According to this model, the TA signal at any time delay and wavelength, $\Delta A(t,\lambda)$, can be reconstructed from superposition of *n*th $C_i(t)$ and $EADS_i(\lambda)$ products,

$$\Delta A(t,\lambda) = \sum_{i=1}^{n} C_i(t) EADS_i(\lambda). \quad [1]$$

$C_i(t)$ is time-dependent concentration of *i*th *EADS* and is expressed as

$$\frac{dC_i(t)}{dt} = k_{i-1}C_{i-1}(t) - k_i C_i(t), i \neq 1, k_{i-1} > k_i, \quad [2]$$

and $C_1(t)$ is populated by the excitation pulse that in spectrometer is represented as IRF:

$$\frac{dC_1(t)}{dt} = IRF(t) - k_1 C_1(t). \quad [3]$$

Global analysis of TRF data included a customized fitting model (target analysis) which assumed more complicated (customized) interactions between compartments. The model used to fit the TRF data is provided in Fig. 2 *B*, *Inset*. Global analysis was performed using CarpetView 1.0 (Light Conversion Ltd.). All plots were created in Origin 2019 (OriginLab Corp.).

Modeling of the Vibronic Progression of Fluorescence Emission Spectrum with FC Factors. Upon assumption that vibronic progression of the fluorescence spectrum is dominated with some average vibronic mode $<\nu>$ with average displacement $<\Delta>$, the FC equation

$$FC(\nu) = C\nu \sum_{\upsilon} \prod_{i} \frac{\Delta_i^{2\upsilon}}{2^{\upsilon}\upsilon!} \exp\left(-\frac{\Delta_i^2}{2}\right) \frac{1}{2\pi\sigma} \exp\left\{-\frac{\left[\nu - \left(\nu_{00} - \sum_i \upsilon\nu_i\right)\right]^2}{2\sigma^2}\right\} \quad [4]$$

simplifies to the following form:

$$FC(\nu) = C\nu \sum_{\upsilon} \frac{\Delta^{2\upsilon}}{2^{\upsilon}\upsilon!} \exp\left(-\frac{<\Delta>^2}{2}\right) \frac{1}{2\pi\sigma} \exp\left(-\frac{\left[\nu - (\nu_{00} - \upsilon<\nu>)\right]^2}{2\sigma^2}\right) \quad [5]$$

where *C* is the scaling constant, υ is the number of vibronic bands included in the progression, σ is the width of the vibronic band (in cm^{-1}), and ν_{00} is (in this case) energy of the S_1 state (in cm^{-1}) of ζ-carotene.

Data Availability. All data needed to support the conclusions of this manuscript are included in the main text and *SI Appendix*. *R. sphaeroides* strains are available upon request.

ACKNOWLEDGMENTS. Spectroscopic work was performed at the Ultrafast Laser Facility of the Center for Solar Energy and Energy Storage at Washington University in Saint Louis. D.M.N. acknowledges the Center for Solar Energy and Energy Storage at McKelvey School of Engineering at Washington University in Saint Louis for financial support. D.J.K.S., D.P.C., C.N.H., and A.H. were supported by the Biotechnology and Biological Sciences Research Council award number BB/M000265/1. C.N.H. further acknowledges award number EP/S002103/1 from the Engineering and Physical Sciences Research Council. A.H. also acknowledges support from a Royal Society University Research Fellowship (award number URF\R1\191548).

1. R. J. Cogdell, H. A. Frank, How carotenoids function in photosynthetic bacteria. *Biochim. Biophys. Acta* **895**, 63–79 (1987).
2. H. A. Frank, T. Polívka, "Energy transfer from carotenoids to bacteriochlorophylls" in *The Purple Phototrophic Bacteria*, C. N. Hunter, F. Daldal, M. Thurnauer, J. T. Beatty, Eds. (Springer, 2009), vol. 28, chap. 12, pp. 213–230.
3. B. E. Kohler, "Electronic structure of carotenoids" in *Carotenoids*, G. Britton, S. Liaaen-Jensen, H. Pfander, Eds. (Spectroscopy, Birkhäuser-Verlag, Basel, 1995), vol. 1B, pp. 3–12.
4. H. Hashimoto, C. Uragami, N. Yukihira, A. T. Gardiner, R. J. Cogdell, Understanding/unravelling carotenoid excited singlet states. *J. R. Soc. Interface* **15**, 20180026 (2018).
5. R. J. Cogdell *et al.*, How carotenoids protect bacterial photosynthesis. *Philos. Trans. R. Soc. Lond. B Biol. Sci.* **355**, 1345–1349 (2000).
6. T. Polívka, H. A. Frank, Molecular factors controlling photosynthetic light harvesting by carotenoids. *Acc. Chem. Res.* **43**, 1125–1134 (2010).
7. Y. Kakitani *et al.*, Conjugation-length dependence of the T_1 lifetimes of carotenoids free in solution and incorporated into the LH2, LH1, RC, and RC-LH1 complexes: Possible mechanisms of triplet-energy dissipation. *Biochemistry* **46**, 2181–2197 (2007).
8. H. Hörvin Billsten *et al.*, Dynamics of energy transfer from lycopene to bacteriochlorophyll in genetically-modified LH2 complexes of *Rhodobacter sphaeroides*. *Biochemistry* **41**, 4127–4136 (2002).
9. J. P. Zhang *et al.*, Mechanism of the carotenoid-to-bacteriochlorophyll energy transfer via the S_1 state in the LH2 complexes from purple bacteria. *J. Phys. Chem. B* **104**, 3683–3691 (2000).
10. A. N. Macpherson, J. B. Arellano, N. J. Fraser, R. J. Cogdell, T. Gillbro, Efficient energy transfer from the carotenoid S_2 state in a photosynthetic light-harvesting complex. *Biophys. J.* **80**, 923–930 (2001).
11. H. Cong *et al.*, Ultrafast time-resolved carotenoid to-bacteriochlorophyll energy transfer in LH2 complexes from photosynthetic bacteria. *J. Phys. Chem. B* **112**, 10689–10703 (2008).
12. F. S. Rondonuwu *et al.*, The role of the $1^1B_u^-$ state in carotenoid-to-bacteriochlorophyll singlet-energy transfer in the LH2 antenna complexes from *Rhodobacter sphaeroides* G1C, *Rhodobacter sphaeroides* 2.4.1, *Rhodospirillum molischianum* and *Rhodopseudomonas acidophila*. *Chem. Phys. Lett.* **390**, 314–322 (2004).

13. D. M. Niedzwiedzki *et al*., Spectroscopic studies of two spectral variants of light-harvesting complex 2 (LH2) from the photosynthetic purple sulfur bacterium *Allochromatium vinosum*. *Biochim. Biophys. Acta* **1817**, 1576–1587 (2012).
14. D. M. Niedzwiedzki *et al*., Functional characteristics of spirilloxanthin and keto-bearing analogues in light-harvesting LH2 complexes from *Rhodobacter sphaeroides* with a genetically modified carotenoid synthesis pathway. *Biochim. Biophys. Acta* **1847**, 640–655 (2015).
15. D. M. Niedzwiedzki, M. Fuciman, M. Kobayashi, H. A. Frank, R. E. Blankenship, Ultrafast time-resolved spectroscopy of the light-harvesting complex 2 (LH2) from the photosynthetic bacterium *Thermochromatium tepidum*. *Photosynth. Res.* **110**, 49–60 (2011).
16. F. Yang *et al*., Excitation dynamics of the light-harvesting complex 2 from *Thermochromatium tepidum*. *Wuli Huaxue Xuebao* **26**, 2021–2030 (2010).
17. J. Koepke, X. Hu, C. Muenke, K. Schulten, H. Michel, The crystal structure of the light-harvesting complex II (B800-850) from *Rhodospirillum molischianum*. *Structure* **4**, 581–597 (1996).
18. S. M. Prince *et al*., Apoprotein structure in the LH2 complex from *Rhodopseudomonas acidophila* strain 10050: Modular assembly and protein pigment interactions. *J. Mol. Biol.* **268**, 412–423 (1997).
19. S. C. Chi *et al*., Assembly of functional photosystem complexes in *Rhodobacter sphaeroides* incorporating carotenoids from the spirilloxanthin pathway. *Biochim. Biophys. Acta* **1847**, 189–201 (2015).
20. D. M. Niedzwiedzki *et al*., New insights into the photochemistry of carotenoid spheroidenone in light-harvesting complex 2 from the purple bacterium *Rhodobacter sphaeroides*. *Photosynth. Res.* **131**, 291–304 (2017).
21. D. M. Niedzwiedzki, C. N. Hunter, R. E. Blankenship, Evaluating the nature of so-called S*-state feature in transient absorption of carotenoids in light-harvesting complex 2 (LH2) from purple photosynthetic bacteria. *J. Phys. Chem. B* **120**, 11123–11131 (2016).
22. P. L. Dilbeck *et al*., Quenching capabilities of long-chain carotenoids in light-harvesting-2 complexes from *Rhodobacter sphaeroides* with an engineered carotenoid synthesis pathway. *J. Phys. Chem. B* **120**, 5429–5443 (2016).
23. R. J. Cogdell, M. F. Hipkins, W. MacDonald, T. G. Truscott, Energy transfer between the carotenoid and the bacteriochlorophyll within the B-800-850 light-harvesting pigment-protein complex of *Rhodopseudomonas sphaeroides*. *Biochim. Biophys. Acta* **634**, 191–202 (1981).
24. A. Angerhofer, F. Bornhauser, A. Gall, R. J. Cogdell, Optical and optically detected magnetic-resonance investigation on purple photosynthetic bacterial antenna complexes. *Chem. Phys.* **194**, 259–274 (1995).
25. H. A. Frank, R. J. Cogdell, Carotenoids in photosynthesis. *Photochem. Photobiol.* **63**, 257–264 (1996).
26. A. Angerhofer, R. J. Cogdell, M. F. Hipkins, A spectral characterization of the light-harvesting pigment-protein complexes from *Rhodopseudomonas acidophila*. *Biochim. Biophys. Acta* **848**, 333–341 (1986).
27. D. Polli *et al*., Carotenoid-bacteriochlorophyll energy transfer in LH2 complexes studied with 10-fs time resolution. *Biophys. J.* **90**, 2486–2497 (2006).
28. M. M. Mendes-Pinto *et al*., Electronic absorption and ground state structure of carotenoid molecules. *J. Phys. Chem. B* **117**, 11015–11021 (2013).
29. M. Fuciman *et al*., Excited state properties of aryl carotenoids. *Phys. Chem. Chem. Phys.* **12**, 3112–3120 (2010).
30. D. M. Niedzwiedzki, L. Cranston, Excited state lifetimes and energies of okenone and chlorobactene, exemplary keto and non-keto aryl carotenoids. *Phys. Chem. Chem. Phys.* **17**, 13245–13256 (2015).
31. R. Bittl, E. Schlodder, I. Geisenheimer, W. Lubitz, R. J. Cogdell, Transient EPR and absorption studies of carotenoid triplet formation in purple bacterial antenna complexes. *J. Phys. Chem. B* **105**, 5525–5535 (2001).
32. D. Kosumi, T. Horibe, M. Sugisaki, R. J. Cogdell, H. Hashimoto, Photoprotection mechanism of light-harvesting antenna complex from purple bacteria. *J. Phys. Chem. B* **120**, 951–956 (2016).
33. D. A. Hartzler *et al*., Triplet excited state energies and phosphorescence spectra of (bacterio)chlorophylls. *J. Phys. Chem. B* **118**, 7221–7232 (2014).
34. C. S. Foote, Y. C. Chang, R. W. Denny, Chemistry of singlet oxygen. X. Carotenoid quenching parallels biological protection. *J. Am. Chem. Soc.* **92**, 5216–5218 (1970).
35. H. Claes, Interaction between chlorophyll and carotenes with different chromophoric groups. *Biochem. Biophys. Res. Commun.* **3**, 585–590 (1960).
36. R. Bensasson, E. J. Land, B. Maudinas, Triplet states of carotenoids from photosynthetic bacteria studied by nanosecond ultraviolet and electron pulse irradiation. *Photochem. Photobiol.* **23**, 189–193 (1976).
37. E. Papagiannakis *et al*., Excited-state dynamics of carotenoids in light-harvesting complexes. 1. Exploring the relationship between the S_1 and S* states. *J. Phys. Chem. B* **110**, 5727–5736 (2006).
38. R. Fujii, K. Onaka, M. Kuki, Y. Koyama, Y. Watanabe, The $2A_g^-$ energies of all-*trans*-neurosporene and spheroidene as determined by fluorescence spectroscopy. *Chem. Phys. Lett.* **288**, 847–853 (1998).
39. C. N. Hunter, G. Turner, Transfer of genes-coding for apoproteins of reaction center and light-harvesting LH1 complexes to *Rhodobacter sphaeroides*. *J. Gen. Microbiol.* **134**, 1471–1480 (1988).
40. I. B. Tikh, M. Held, C. Schmidt-Dannert, BioBrick™ compatible vector system for protein expression in *Rhodobacter sphaeroides*. *Appl. Microbiol. Biotechnol.* **98**, 3111–3119 (2014).
41. D. J. K. Swainsbury *et al*., Engineering of B800 bacteriochlorophyll binding site specificity in the *Rhodobacter sphaeroides* LH2 antenna. *Biochim. Biophys. Acta Bioenerg.* **1860**, 209–223 (2019).
42. D. M. Niedzwiedzki *et al*., Carotenoid-induced non-photochemical quenching in the cyanobacterial chlorophyll synthase-HliC/D complex. *Biochim. Biophys. Acta* **1857**, 1430–1439 (2016).
43. D. M. Niedzwiedzki, J. Jiang, C. S. Lo, R. E. Blankenship, Low-temperature spectroscopic properties of the peridinin-chlorophyll a-protein (PCP) complex from the coral symbiotic dinoflagellate *Symbiodinium*. *J. Phys. Chem. B* **117**, 11091–11099 (2013).
44. D. M. Niedzwiedzki, H. Liu, R. E. Blankenship, Excitation energy transfer in intact CpcL-phycobilisomes from *Synechocystis* sp. PCC 6803. *J. Phys. Chem. B* **123**, 4695–4704 (2019).
45. I. H. M. van Stokkum, D. S. Larsen, R. van Grondelle, Global and target analysis of time-resolved spectra. *Biochim. Biophys. Acta* **1657**, 82–104 (2004).